Studies of the Phase Transitions, Structure, and Dynamics for Main-Chain Thermotropic Liquid Crystalline Polyethers and Polyurethanes with the Same Mesogen and Spacer Units

Miwa Murakami, Hiroyuki Ishida, Masayuki Miyazaki, Hironori Kaji, and Fumitaka Horii*

Institute for Chemical Research, Kyoto University, Uji, Kyoto 611-0011, Japan

Received December 15, 2002; Revised Manuscript Received March 3, 2003

ABSTRACT: Phase transition behavior, structure, and dynamics have been investigated for main-chain thermotropic liquid crystalline polyethers (EDMB-10) and polyurethanes (UDMB-10) with the same mesogen and spacer units by mainly using DSC and solid-state ^{13}C NMR spectroscopy. The liquid crystallization temperature (T_{lc}), which corresponds to the isotropic melt → nematic phase transition temperature determined by DSC, is found to stay almost constant irrespective of the cooling rate from the isotropic melt for EDMB-10 while the crystallization temperature (T_c) greatly decreases with increasing cooling rate. This fact leads to the preparation of the liquid crystalline glass by quenching from the isotropic melt to ice−water. In contrast, T_{lc} and T_c for UDMB-10 are observed as an overlapped single exothermic peak in DSC, and both temperatures are found to significantly depend on the cooling rate. This fact suggests that somewhat larger-scale reorientation of the mesogen and spacer units, which may result in the formation of segmental assemblies through intermolecular hydrogen bonding, are inevitable for the liquid crystallization from the isotropic melt in the case of UDMB-10. The CSA spectra of the respective carbons for the mesogen and spacer units, which were successfully measured by the MAT method, have been elucidated in detail to characterize molecular motion of the constituent units in the EDMB-10 and UDMB-10 samples that were crystallized from the isotropic melt through the nematic phase: The mesogen units are found to be in the rigid state or undergo restricted fluctuation with amplitudes less than ±20° in the crystalline and noncrystalline regions for both samples. In contrast, the CH_2 sequences are subjected to much enhanced motion such as cooperative $t-g$ exchanges or the thermal fluctuation around chain axis with the planar zigzag conformation in the crystalline region for EDMB-10 or UDMB-10, respectively. Interestingly, similar cooperative $t-g$ exchange motion is also allowed to occur for the noncrystalline CH_2 sequences in UDMB-10 whereas the corresponding CH_2 units adopt random conformation in EDMB-10. On the basis of these experimental results, the structural models have been proposed for the nematic phase in EDMB-10 and UDMB-10.

Introduction

On account of excellent mechanical, optical, and thermal properties, main-chain thermotropic liquid crystalline polymers have drawn both scientific and industrial attention.[1−6] A large number of main-chain thermotropic liquid crystalline polymers with a variety of structural features and interconnecting units between the mesogenic groups and the flexible or rigid spacers were synthesized and characterized by different methods in these two decades, and some of them have successfully been developed to commercialized products in addition to main-chain lyotropic aramides developed much earlier. However, there is still only limited information about the relationship between the chemical structure and properties in the main-chain thermotropic liquid crystalline polymers, probably due to thermal instability in the liquid crystalline phase for most of polymers. We have recently synthesized liquid crystalline (LC) polyurethane and polyether with the same mesogen and spacer units and mainly characterized the crystalline−noncrystalline structure and the spacer conformation for the samples that were crystallized by slowly cooling from the isotropic melt through the nematic phase.[6,7] As a result, the spacer CH_2 sequences have been found to adopt greatly different conformations for these two polymers in both crystalline and noncrystalline regions although the crystalline−noncrystalline structure is not so different for them.

In this paper, therefore, the phase transitions concerning liquid crystallization[8] and crystallization and molecular motions of the mesogen and spacer units are characterized in detail for the LC polyether and polyurethane with different molecular weights by mainly using DSC and solid-state ^{13}C NMR spectroscopy. On the basis of these experimental results, structural models of the LC phases are proposed for these LC polymers by considering the existence or absence of the intermolecular hydrogen bonding. The formation of the LC glassy phase for EDMB-10 and a new crystal form produced from that phase will be reported elsewhere in the near future.

Experimental Section

Samples. Most reagents and solvents except for 3,3′-dimethyl-4,4′-biphenyldiyl diisocyanate (from Nippon Soda Co., Ltd.) and *o*-tolidine (from Tokyo Chemical Industry Co., Ltd.) were purchased from Nakalai Tesque in Kyoto. These materials were used without further purification.

Polyurethanes UDMB-10 (Scheme 1) with different molecular weights were polymerized in anisole at 140 °C for 6 h with 3,3′-dimethyl-4,4′-biphenyldiyl diisocyanate as mesogen, 1,10-dodecanediol as spacer, and 1-hexanol as molecular weight controller.[7,10] M_ns of the UDMB-10 samples, which were determined by the end-group analyses using solution-state ^1H NMR spectroscopy, were 3000, 6500, and 16 800. On the other hand, polyethers EDMB-10 (Scheme 1) were synthesized in a two-phase system which was composed of 3 N NaOH aqueous solution containing 3,3′-dimethyl-4,4′-dihydroxy-biphenyl and

10.1021/ma025963s CCC: $25.00
Published on Web 05/09/2003

Scheme 1. Chemical Structure of LC Polyether (EDMB-10) and Polyurethane (UDMB-10)

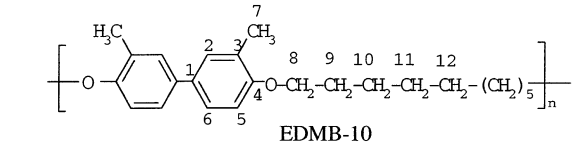

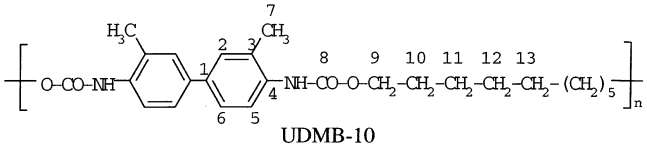

o-dichlorobenzene having 1,10-dibromodecane at 93 °C for 6 h under an argon atmosphere with vigorous stirring by using tetra-*n*-butylammonium hydrogen sulfate as a phase transfer catalyst.[9] Here, 3,3′-dimethyl-4,4′-dihydroxybiphenyl was synthesized from *o*-tolidine via its diazonium chloride.[7] M_ns of the EDMB-10 samples determined by polystyrene-calibrated GPC were 6900−72 000, and their M_w/M_n values were as somewhat broad as 2.0−5.6.

As for EDMB-10, molecular weight fractionations were carried out two times at 50 and 40 °C by the fractional precipitation method using *o*-dichlorobenzene and methanol as solvent and precipitant, respectively. A total of eight fractions were obtained in each fractionation, and five fractions with $M_n = 5500-50\,000$ and $M_w/M_n = 1.3-1.8$ and other seven fractions with $M_n = 2700-23\,000$ and $M_w/M_n = 1.1-1.4$ were used in this work.

Differential Scanning Calorimetry (DSC). The thermal transition behavior of each sample was measured on a TA Instruments DSC2910 differential scanning calorimeter. The temperature was calibrated using indium. All DSC runs were performed for 2.2−10.5 mg under a nitrogen atmosphere at scanning rates of 0.1−20 °C/min. A first-order transition temperature was measured as a maximum or minimum of each transition peak.

Optical Microscopy. A Nikon OPTIPHOT2-POL optical polarizing microscope equipped with a Linkam LK-600PM hot stage was used to observe thermal phase transition and texture changes. Each powderlike sample was placed on a glass slide, covered with a glass coverslip, and heated or cooled under a nitrogen atmosphere in the hot stage at a rate of 10 °C/min.

Solid-State ^{13}C NMR Measurements. Solid-state ^{13}C NMR measurements were carried out at room temperature on a JEOL JNM-GSX200 or Chemagnetics CMX-200 spectrometer equipped with a JEOL variable temperature magic angle spinning (MAS) system operating at 50.0 MHz under a static magnetic field of 4.7 T. ^{1}H and ^{13}C radio-frequency fields $\gamma B_1/2\pi$ were 62.5 kHz. The contact time for the CP process was 1.0 ms, and the recycle time after the acquisition of each free induction decay (FID) was 5 s throughout this work. The MAS rate was set to 3.6 kHz in order to avoid the overlapping of spinning sidebands on other resonance lines. ^{13}C chemical shifts were expressed as values relative to tetramethylsilane (Me_4Si) by using the CH_3 line at 17.36 ppm of hexamethylbenzene crystals as an external reference. ^{13}C spin−lattice relaxation times (T_1^C) were measured by using the CPT1 pulse sequence.[11]

^{13}C chemical shift anisotropy (CSA) spectra were measured at room temperature by the two-dimensional magic angle turning (MAT) method[12,13] on a Chemagnetics CMX-400 spectrometer under a static magnetic field of 9.4 T. ^{1}H and ^{13}C radio-frequency field strengths $\gamma B_1/2\pi$ were 62.5 kHz, and the MAS rate was precisely adjusted to be 130 ± 1 Hz for EDMB-10 and 127 ± 1 Hz for UDMB-10.

Results and Discussion

Phase Transition Behavior. Figure 1 shows DSC cooling and heating thermograms for the EDMB-10 sample with $M_n = 10\,000$ at a scanning rate of 10 °C/min. In both first cooling and second heating processes, two phase transition peaks are evidently observed, and the nematic phase was found to appear between the two peaks in each process by an optical polarizing microscope. Similar DSC thermograms were also obtained for EDMB-10 with a smaller molecular weight (M_n = 8540),[7] but the temperature ranges for the nematic phase were significantly wider compared to those for the present sample. This fact indicates that these phase transitions will depend on molecular weight for EDMB-10 and thus probably also on the cooling and heating rates.

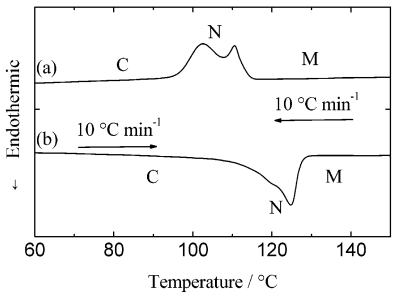

Figure 1. DSC thermograms of EDMB-10 recorded on cooling (a) and heating (b) at a rate of 10 °C/min.

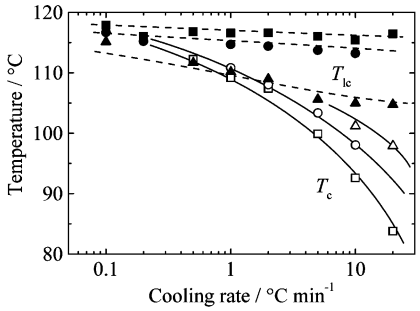

Figure 2. Plots of liquid crystallization temperatures (T_{lc}) and crystallization temperatures (T_c) observed on the cooling process as a function of the cooling rate for EDMB-10 with different molecular weights: triangles, M_n = 7000; circles, M_n = 10 000; squares, M_n = 72 000.

Figure 2 shows dependences of the liquid crystallization[8] temperature (T_{lc}) and crystallization temperature (T_c) on the cooling rate for three EDMB-10 samples with different molecular weights. Here, T_{lc} and T_c are the peak temperatures for the isotropic melt → liquid crystalline phase and the liquid crystalline phase → crystalline phase transitions observed in the cooling process on DSC thermograms, as seen in Figure 1, respectively. The T_{lc}s seem to be almost independent of the cooling rate for higher molecular weights, although the slight decrease in T_{lc} is observed with increasing cooling rate for a lower molecular weight. In contrast, the T_c is remarkably decreased with increasing cooling rate, and the extent of the decrease is much enhanced for higher molecular weights. Such a difference in cooling rate dependence between T_{lc} and T_c may be associated with the difference in reorientation process for the mesogen and spacer units between liquid crystallization and crystallization for EDMB-10. This problem will be discussed later using a structural model. In addition, it should be noted here that the LC glass is readily produced by quenching each EDMB-10 sample from the isotropic melt into ice−water as a result of rapid cooling in which crystallization is completely hindered while liquid crystallization is still allowed to

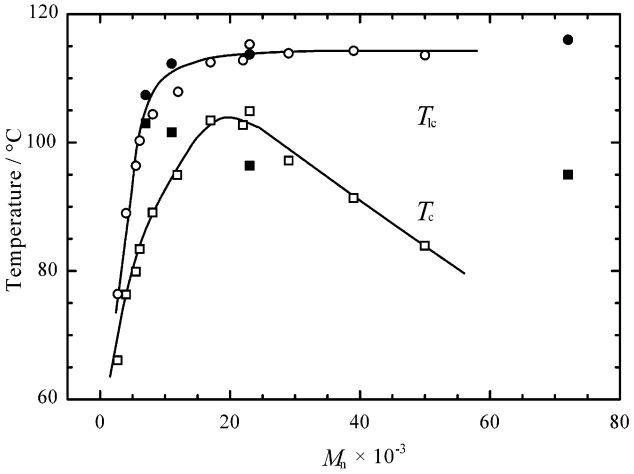

Figure 3. Plots of liquid crystallization temperatures (T_{lc}) and crystallization temperatures (T_c) observed on the cooling process as a function of the molecular weight for EDMB-10: open symbols, fractionated; closed symbols, unfractionated.

occur. The structure and properties of the LC glass of EDMB-10 thus produced will be reported elsewhere.

To examine the molecular weight dependences of T_{lc} and T_c, DSC thermograms were also measured for different molecular weight fractions of EDMB-10 at a cooling rate of 10 °C/min. In Figure 3, the T_{lc} and T_c thus obtained are plotted against M_n together with the corresponding data for four unfractionated EDMB-10 samples with different M_ns. As is clearly seen, the T_{lc} is drastically increased with increasing molecular weight and tends to level off for M_ns higher than about 20 000. Such leveling off of T_{lc} may be interpreted by the same factor associated with mesogen reorientation as the case of no cooling rate dependence of T_{lc} shown in Figure 2. In contrast, a maximum appears for the M_n dependence of T_c: The T_c is greatly decreased with increasing M_n for M_ns higher than about 20 000, although it is initially increased in a similar way as the case of T_{lc}. This fact is also related to the large dependence of T_c on the cooling rate, suggesting the higher restriction of crystallization probably due to slower reorientation of polymer chains. Moreover, it should be noted that there is also a large difference in effect of molecular weight distribution between T_{lc} and T_c: The T_{lc}s of unfractionated samples with $M_w/M_n = 2.6-3.2$ are found to be in good accord with those for fractionated samples with $M_w/M_n = 1.2-1.8$, probably reflecting no dependence of T_{lc} on the molecular weight. However, T_cs for the unfractionated samples are greatly deviated from those for the fractionated samples, particularly in the higher molecular weight region. Nucleation of crystallization may be promoted in unfractionated samples with higher M_ns by the presence of molecular weight fractions with M_ns ($\sim$20 000) around the maximum observed in Figure 3. Similar molecular weight dependencies of T_{lc} and T_c were frequently observed for unfractionated samples such as polyesters[1,3,14] and other types of polyethers,[1,3,15] but to our knowledge, there is no report to demonstrate such an evident effect of the fractionation on T_c, as shown in Figure 3.

As for the heating process shown in Figure 1, the structure produced in the cooling process will greatly depend on the phase transition behavior. In fact, preliminary DSC measurements indicated that the DSC endothermograms significantly depend on the heating rate as well as the cooling rate. Since the characterization of the heating process seems to be more complicated, only the cooling process is treated in this work.

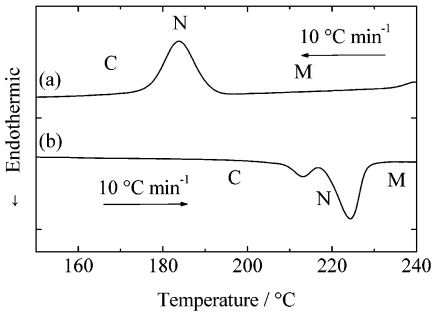

Figure 4. DSC thermograms for UDMB-10 recorded on cooling at a rate of 10 °C/min.

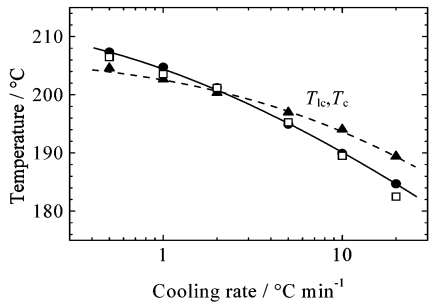

Figure 5. Plots of liquid crystallization temperatures (T_{lc}) and crystallization temperatures (T_c) observed on the cooling process as a function of the cooling rate for UDMB-10 with different molecular weights: triangles, $M_n = 3000$; circles, $M_n = 6500$; squares, $M_n = 16\,800$.

Figure 4 shows DSC thermograms of unfractionated LC polyurethane UDMB-10 with $M_n = 6500$ measured in the cooling and heating processes at a scanning rate of 10 °C. The molecular weight distribution could not be determined because of a lack of a solvent suitable for GPC. Interestingly, a single exothermic peak is observed in the cooling process from the isotropic melt whereas two endothermic peaks appear in the subsequent heating process. This result is in good accord with the previous result observed for the UDBM-10 sample with $M_n = 11\,700$,[6] although the transition temperatures seem to be somewhat different probably depending on molecular weight and scanning rate. It was also reconfirmed in this sample by an optical polarizing microscopic observation that the nematic phase first appears in each domain in the cooling process, and subsequent crystallization occurs without a significant delay. As a result, liquid crystallization and crystallization are detected as completely superposed processes on the DSC thermogram, giving the same T_{lc} and T_c.

In Figure 5, T_{lc} and T_c are plotted against the cooling rate for UDMB-10 with different molecular weights. In the ranges of molecular weight and cooling rate shown here, T_{lc} and T_c are always superposed with each other, and they are markedly decreased with increasing cooling rate. This fact indicates that liquid crystallization is also induced depending on the cooling rate as well as molecular weight unlike the case of EDMB-10, suggesting the necessity of some reorientation associated with larger size of structural entities even for liquid crystallization in UDMB-10. It should be additionally noted here that less solubility of UDBM-10 makes difficult the synthesis of higher molecular weight samples. DSC measurements at slower cooling rates were also impossible because of thermal instability of this polymer with

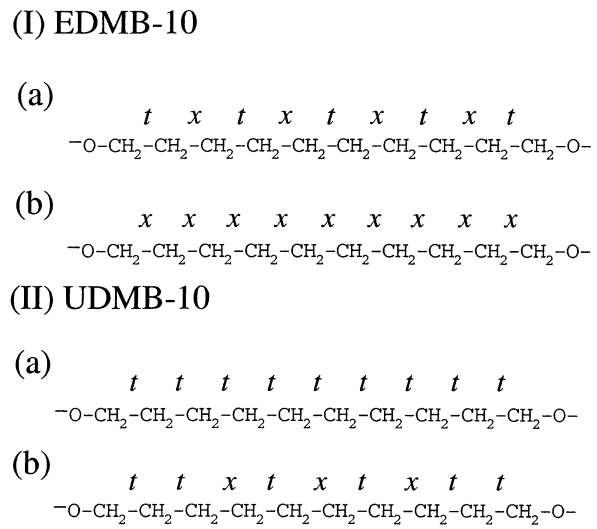

Figure 6. Chain conformations for the spacer CH_2 sequences in different components in the EDMB-10 and UDMB-10 samples which were crystallized by slowly cooling from the isotropic melt through the nematic phase: (a) crystalline and medium; (b) noncrystalline. *t* and *x* indicate *trans* and *trans*−*gauche* exchange conformations, respectively.

urethane bonds. Therefore, further experiments could not be carried out from these limitations for UDMB-10.

Conformation of the Spacer Methylene Sequences. In both EDMB-10 and UDMB-10 samples which were crystallized by slowly cooling from the isotropic melt through the LC phase, their ^{13}C spin−lattice relaxation processes were characterized for the spacer CH_2 carbons as previously reported in detail.[6,7] As a result, it was found that there are three components with different T_1^C values, which are assigned to the crystalline, medium, and noncrystalline components in the order of decreasing T_1^C, in the respective samples with different M_ns. Here, the noncrystalline component should be regarded as the supercooled LC component because this component is left as liquid crystalline component in those samples even at room temperature after the crystallization from the LC state at a higher temperature.

By using such differences in T_1^C, the CP/MAS ^{13}C NMR spectrum of each component was separately recorded, and the line shape analysis was performed for each component spectrum thus obtained for the CH_2 sequences. Since the analytical method was described in detail in our previous papers,[6,7,9] a brief description is made here: In this analysis a 2.5 ppm upfield shift was assumed to occur for a resonance line of a specific CH_2 carbon as a result of the half effect of the conventional γ-gauche effect[16] when the *trans*−*gauche* exchange conformation is induced in the planar zigzag CH_2 sequence, and all spectra were successfully analyzed under this assumption as previously reported in detail.[6,7,9] The chain conformations of the spacer CH_2 sequences could be definitely determined by the evaluation of chemical shift values thus obtained for the respective components in the EDMB-10 and UDMB-10 samples, and they are summarized in Figure 6. In EDMB-10, the crystalline and medium components adopt the alternate *txtxtxtxt* conformation whereas the supercooled LC component has a rather random chain conformation described as *xxxxxxxxx* like that at the isotropic melt or in solution. Here, *t* and *x* indicate the *trans* and *trans*−*gauche* exchange conformations, respectively. In contrast, the supercooled LC component in UDMB-10 adopts partially alternate chain conformation *ttxtxtxtt* while the crystalline and medium components are in the planar zigzag conformation.

A separate molecular dynamics simulation revealed that the characteristic *txtxtxtxt* conformation for EDMB-10 is well reproduced above about 400 K in the crystalline state.[17] In this simulation, Cerius[2] (Version 4.2 MatSci., Molecular Simulations Inc.) was utilized with the PCFF force field.[18] Sixteen EDMB-10 chains composed of five mesogen units and four spacer sequences were set in an appropriate cell under two-dimensional periodic boundary conditions in the lateral direction. The initial structure was produced by the energy minimization at 100 K, and the cell parameters obtained were almost in accord with the unit cell parameters estimated by the WAXS analysis for the uniaxially drawn EDMB-10 sample separately prepared. According to the evaluation of the time trajectory of the spacer conformation, a coupled *g* and *g′* introduction was found to occur at random in the two bonds of the C−C bonds that are described as *x* in the *txtxtxtxt* conformation. Moreover, the torsion angles of the $O-CH_2$ bonds at the terminals of the spacer sequence were changed from 90° to 180° cooperatively with the introduction of the *g* and *g′* conformations. As a result, the cell length along the chain axis stays almost constant irrespective of the rapid coupled *t*−*g* and *t*−*g′* transition in this crystalline state. More detailed discussion will be made elsewhere after the characterization of the molecular motion of the mesogen units.

As for UDMB-10, such a MD simulation was not performed in detail because it was impossible to create the liquid crystalline phase at any temperature by this simulation and to examine the possibility of the partially alternate chain conformation *ttxtxtxtt* in that phase. Nevertheless, the MD simulation results of EDMB-10 suggest that the existence of the *txtxtxt* sequence may be also due to preferential orientation of the mesogen groups even in the supercooled LC state for UDMB-10, similar to the case of the crystalline state for EDMB-10. A possible structural model will be some kind of segmental assemblies through intermolecular hydrogen bonding between the NH and CO groups as described later. In fact, natural abundant ^{15}N NMR measurements confirmed the formation of the intermolecular hydrogen bonding in the supercooled LC component as well as in the crystalline region for UDMB-10.[6]

Molecular Motion of the Mesogen and Spacer Units As Revealed by CSA. In contrast to the cases of the spacer CH_2 sequences of EDMB-10 and UDMB-10, the mesogen carbons were found to have two different T_1^C values at room temperature for the samples crystallized from the isotropic melt through the LC phase.[6,7] This fact implies that the discrimination among the crystalline, medium, and noncrystalline components may be not fully made for the mesogen units probably because of their low molecular mobility. Namely, since the mesogen units have bulky and rigid structure, molecular mobility may not be highly enhanced even in the noncrystalline region while the CH_2 sequences undergo much more rapid conformational changes. As a result, such mesogens will be detected through the T_1^C measurements simply as two components with more and less molecular mobilities.

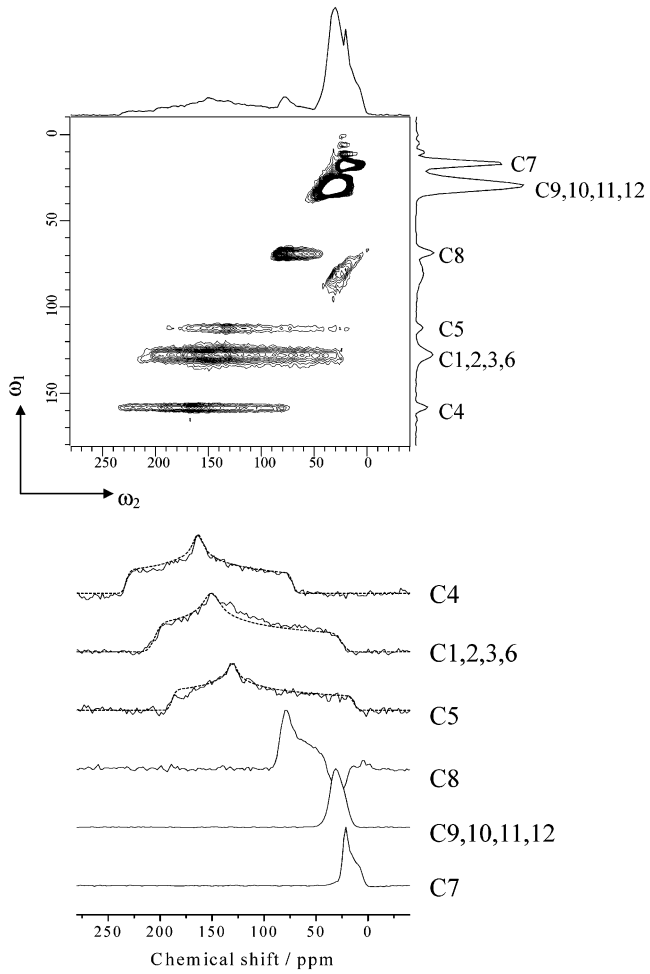

Figure 7. 2D MAT ^{13}C NMR spectrum measured at room temperature for the EDMB-10 sample with $M_n = 12\,000$ and ^{13}C CSA spectra obtained as slices along the ω_2 axis for the respective carbons. Broken lines are CSA spectra simulated for the phenylene carbons in the rigid state.

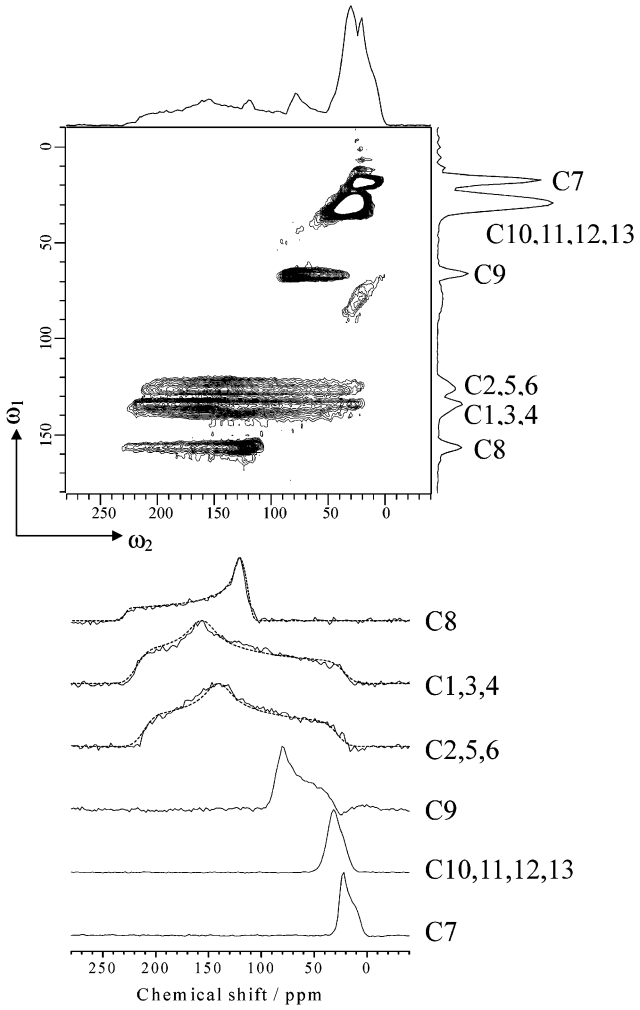

Figure 8. 2D MAT ^{13}C NMR spectrum measured at room temperature for the UDMB-10 sample with $M_n = 11\,700$ and ^{13}C CSA spectra obtained as slices along the ω_2 axis for the respective carbons. Broken lines are CSA spectra simulated for the phenylene and carbonyl carbons in the rigid state.

Figures 7 and 8 respectively show two-dimensional MAT ^{13}C NMR spectra measured at room temperature for the EDMB-10 and UDMB-10 samples crystallized from the isotropic melt through the LC phase and the CSA spectra obtained as slices along the ω_2 axis for the respective isotropic resonance lines. It is found that the CSA spectra are successfully measured for both samples by the MAT method. In particular, there is no deformation of the CSA line shape due to spinning sidebands in this method although it is a serious problem in the case of the switching angle sample spinning (SASS) method employing a normal spinning rate.[9,19,20] It should be noted here that the artifacts with minus intensities appearing near the C8 contribution may be the axial peaks produced at the center of the ω_1 dimension probably due to instability of sample spinning.[21] In these figures the simulated CSA spectra in the rigid state are also shown for the aromatic and carbonyl carbons as broken lines.

These simulated spectra are found to be in good accord with the observed CSA spectra for each sample, although some minor deviation appears in the overlapped CSA spectra for several carbon species. However, it should be noted that the constituent Gaussian curves used for the simulation, which correspond to the resonance lines for the ^{13}C nuclei located at the respective positions in each powdered sample, have different line widths for EDMB-10 (3 ppm) and for UDMB-10 (8 ppm). This fact indicates that the local structure may be more widely distributed for UDMB-10 than for EDMB-10. Although the aromatic and carbonyl carbons in each sample contain at least two components with different T_1^Cs as described above, there seems to be almost no difference in CSA between these two components. This fact may suggest that the phenylene ring will be highly hindered in molecular mobility even in the noncrystalline region as well as in the crystalline region. However, the T_1^C values are as short as 3−8 s for EDMB-10 or 11−19 s for UDMB-10 in the noncrystalline region, whereas they are 12−30 s for EDMB-10 or 190−210 s for UDMB-10 in the crystalline region.[6,7,9] Therefore, the phenylene rings will undergo rapid fluctuation with rather small amplitudes mainly around the phenylene bond axis in the noncrystalline region in both samples and also at a somewhat lower level even in the crystalline region for EDMB-10. In fact, a previous simulation[9,22] assuming the two-site exchange model revealed that the CSA line shape of the aromatic CH carbon is not significantly altered from the powder pattern in the rigid state even when the phenylene ring undergoes the flip motion with the flip angle less than about 20° around the bond axis.

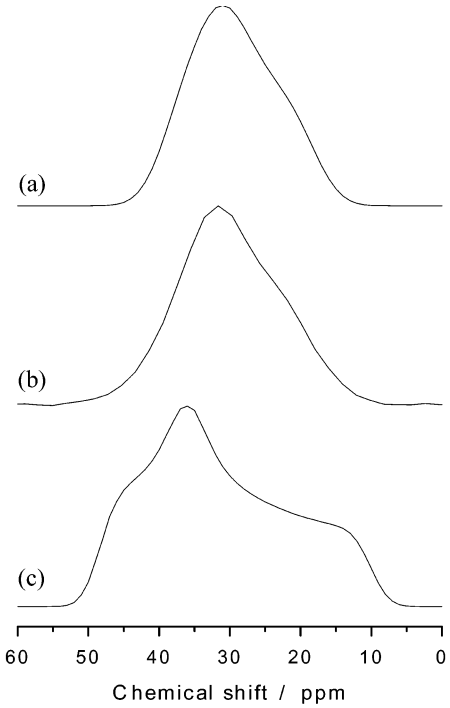

Figure 9. Enlarged CSA spectra of the CH_2 carbons for the EDMB-10 (a) and UDMB-10 (b) samples, which are originally shown as slices along the ω_2 axis in Figures 7 and 8, respectively. (c) CSA spectrum simulated for polyethylene crystals with the isotropic chemical shift value of 32.0 ppm.[28−30]

The slice spectra of the OCH_2 and CH_3 carbons also show other types of clear chemical shift anisotropies in both samples. Since the MAS-averaged isotropic chemical shifts of these carbons are almost the same for the crystalline and noncrystalline components, there may be also no difference in CSA between the two components. As for the OCH_2 carbons, the σ_{11} and σ_{22} values in the rigid state are equal for poly(ethylene terephthalate)[23,24] or not so greatly different from each other for poly(ethylene oxide).[23,25] It seems, therefore, difficult to obtain information about molecular motion from these CSA spectra even if the OCH_2 carbons are subjected to thermal fluctuation or flip motion around the σ_{33} axis. In contrast, the CSA spectra of the CH_3 carbons are axially symmetric in both samples whereas they are typical powder patterns with different principal values for toluene[23,26] and *p*-xylene[23,27] in the rigid state. This fact implies that each CH_3 group may rapidly rotate in the crystalline and noncrystalline regions. Moreover, the thermal fluctuation of the phenylene ring may be somewhat superposed on the CH_3 rotation because the axially symmetric CSA spectra seem to significantly narrow in both samples.

In contrast, CSAs for the CH_2 lines seem to be much averaged in the scale of these figures. To confirm such partial averaging, enlarged CSA spectra for the CH_2 carbons are shown in Figure 9 together with the rigid CSA pattern simulated for the CH_2 carbon in the polyethylene crystals by using the reported principal values.[28−30] In these three spectra the positions of their isotropic chemical shifts are set to 32.0 ppm, which corresponds to the chemical shift value at the peak top for the crystalline CH_2 line experimentally obtained for EDMB-10 or UDMB-10 by MAS. Since both observed lines contain contributions from several CH_2 carbons, it is difficult to obtain information about real CSA line shape for each CH_2 carbon from these spectra: For example, the upfield shoulders appearing in both spectra may not be residual CSA contributions but the contributions from the carbons with different isotropic chemical shifts. Nevertheless, these two spectra are found to be much narrower than the CSA spectrum of polyethylene crystals.[28−30] Such narrowing may be due to the rapid conformational changes for the CH_2 spacer sequences in both crystalline and noncrystalline regions for EDMB-10 as described above. In the case of UDMB-10, however, the CH_2 sequences adopt the planar zigzag conformation in the crystalline region for UDMB-10 as shown in Figure 6, whereas they also undergo rapid conformational changes in the noncrystalline region. Since the CSA spectrum for the CH_2 carbons is also found to be much narrower in UDMB-10, the CH_2 sequence with the planar zigzag conformation will be subjected to the random fluctuation around the chain axis with rates of more than about 10^3 s^{-1} even in the crystalline region.

Structural Models for the Liquid Crystalline State. On the basis of the experimental results described above, we propose the structural models schematically representing the liquid crystalline state for EDMB-10 and UDMB-10 as shown in Figure 10. In the case of EDMB-10, each mesogen group will be uniaxially oriented rather easily without any long-range rearrangement of molecular chains to form the nematic phase when the system is cooled from the isotropic melt. This situation may be reflected on almost no cooling rate dependence or no molecular weight dependence of the liquid crystallization temperature as seen in Figure 2 or Figure 3, respectively. The spacer CH_2 sequences are not highly restricted in conformation but subjected to rather random $t-g$ transitions for the respective C−C bonds. Nevertheless, the mesogen groups are highly hindered in molecular motion and undergo the thermal fluctuation with amplitudes less than about ±20° around the phenylene bond axis. Such reduced molecular mobility and uniaxial orientation of the mesogen groups may affect the molecular motion of the CH_2 sequences, and the respective $t-g$ exchange motions will not be completely independent but somewhat cooperative although the details cannot be characterized by the present NMR method. Some amount of chain folds should be also considered as reported in the smectic phase of liquid crystalline polyester,[31] although they are neglected here for simplicity. According to this structural model, the remarkable cooling rate dependence of the crystallization temperature, which was observed in Figure 2, can be well interpreted in terms of the necessity of time for rather long-range rearrangements of molecular chains from the nematic phase to the crystalline phase.

In the liquid crystalline phase for UDMB-10, some sort of segmental assemblies will be formed through intermolecular hydrogen bonding between the NH and CO units as shown in Figure 10, and these assemblies may be uniaxially oriented to form the nematic phase like the mesogens in the case of EDMB-10. Since the long-range rearrangement of molecular chains is inevitable for the formation of such segmental assemblies in this case, the liquid crystallization temperature markedly depends on the cooling rate as shown in Figure 5. After the formation of the assemblies, minor local structural modification may be enough for the crystallization, which leads to rapid crystallization following the liquid crystallization as detected a single

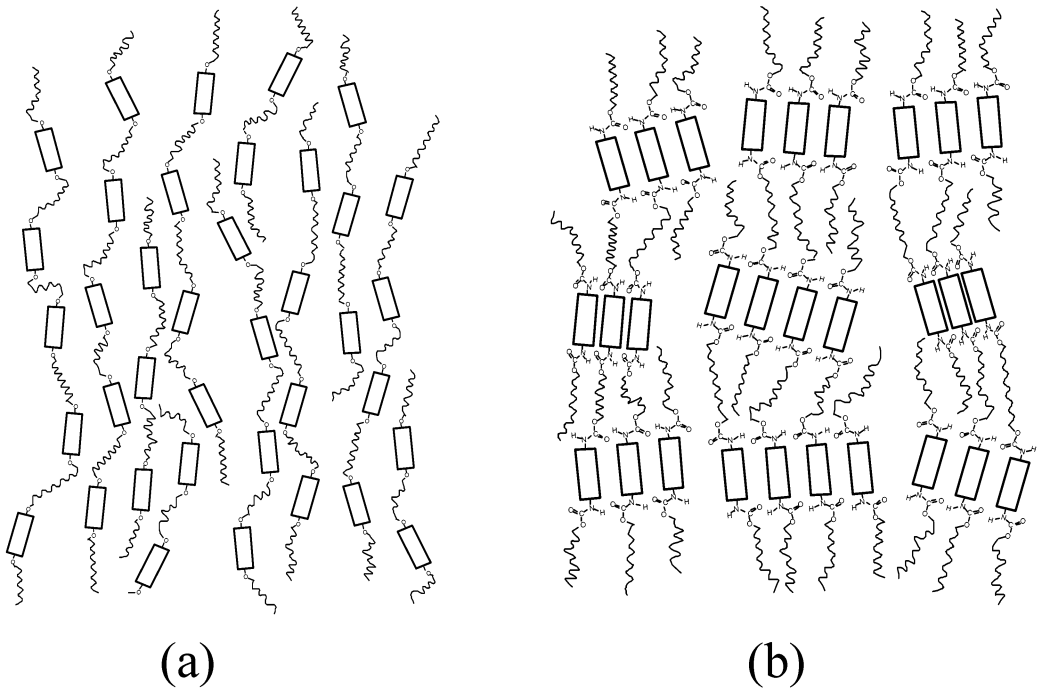

Figure 10. Schematic structural models for the nematic phases in EDMB-10 (a) and UDMB-10 (b).

exothermic peak in the cooling process from the isotropic melt as shown in Figure 4. Since the liquid crystalline state cannot be stably kept for a certain period by this reason, it would be impossible to confirm the segmental assemblies by a spectroscopic or diffractometric method. Nevertheless, the characteristic spacer chain conformation of the noncrystalline component for UDMB-10 shown in Figure 6 will also support the formation of the segmental assemblies in the liquid crystalline state: Namely, the respective spacer CH_2 sequences are fixed at the ends to the aggregated mesogens that are rather oriented parallel to the director in each domain forming the nematic phase. In that case, even if a gauche (g) is introduced in a certain C−C bond, another gauche (g') with a minus torsion angle should be cooperatively formed in the same CH_2 sequence to keep the chain axis almost constant. Accordingly, the *ttxtxtxtt* conformation observed for UDMB-10 could be interpreted in terms of the introduction of such paired g and g' in the C−C bonds indicated by x. In fact, our recent MD simulation[32] revealed that paired g and g' conformations are generated in specified alternate C−C bonds along the CH_2 sequence for EDMB-10 in the crystalline region where the molecular chain axis should be more strictly fixed compared to the case in the nematic phase for UDMB-10.

Conclusions

We have investigated phase transition behavior, structure, and molecular motion for liquid crystalline polyethers (EDMB-10) and polyurethanes (UDMB-10) with the same mesogen and spacer units by mainly employing DSC and solid-state ^{13}C NMR spectroscopy and obtained the following conclusions:

(1) In the case of EDMB-10, the liquid crystallization temperature T_{lc} is found to be almost independent of the cooling rate from the isotropic melt whereas the crystallization temperature T_c greatly depends on the rate. Molecular weights do not also affect T_{lc} for the M_n fractions more than about 20 000, while T_c is significantly decreased after going over the maximum around 20 000 with increasing molecular weight. These facts suggest that minor local reorientation of the mesogen and spacer groups may be enough to form the nematic phase from the isotropic melt for EDMB-10, whereas rather long-range reorganization of the segments should be inevitable for the crystallization from the nematic phase.

(2) T_{lc} and T_c are completely superposed upon each other for UDMB-10, and both temperatures significantly depend on the cooling rate and also on molecular weight. This may be due to the fact that somewhat larger-scale reorganization will be necessary even for the creation of the nematic phase probably because of the formation of some kind of segmental assemblies through intermolecular hydrogen bonding in the nematic phase for UDMB-10. In contrast, the crystallization should occur without appreciable delay after the formation of such segmental assemblies in the nematic phase.

(3) ^{13}C chemical shift anisotropies (CSA) have successfully been measured for the constituent carbons in the EDMB-10 and UDMB-10 samples crystallized from the isotropic melt through the nematic phase by the MAT method. The evaluation of the CSA spectra reveals that the mesogen units are in the rigid state or undergo thermal fluctuation with amplitudes less than ±20° around the phenylene bond axis in the crystalline and noncrystalline regions for both samples. In contrast, the CH_2 units in the spacers are subjected to the specific cooperative $t-g$ exchange motions or rather restricted fluctuation around the planar zigzag chain axis in the crystalline region for EDMB-10 or UDMB-10, respectively. Moreover, the CH_2 sequences in the noncrystalline region seem to adopt a random conformation in EDMB-10, whereas they undergo a similar type of cooperative $t-g$ exchange motion in UDMB-10.

(4) On the basis of these results, structural models have been proposed for the nematic phases in EDMB-10 and UDMB-10: The respective mesogen groups should be uniaxially oriented in each domain for EDMB-

10 without significant restriction while the spacer CH_2 sequences will adopt rather random conformation. In contrast, some kind of segmental assemblies may be formed through intermolecular hydrogen bonding between the NH and CO groups for UDMB-10, and the CH_2 sequences are appreciably hindered in conformation and molecular mobility.

Acknowledgment. This work was supported by Grant-in-Aid for Scientific Research (No. 12450384) from the Ministry of Education, Culture, Sports, Science and Technology, Japan.

References and Notes

(1) Ciferri, A., Ed. *Liquid Crystallinity in Polymers. Principles and Fundamental Properties*; VCH Publ.: New York, 1991.
(2) Isayev, A. I., Kyu, T., Cheng, S. Z. D., Eds. *Liquid-Crystalline Polymer Systems. Technological Advances*; ACS Symposium Series 632; American Chemical Society: Washington, DC, 1996.
(3) Collings, P. J., Patel, J. S., Eds. *Handbook of Liquid Crystal Research*; Oxford University Press: New York, 1997.
(4) Ward, I. M., Ed. *Structure and Properties of Oriented Polymers*; Chapman & Hall: London, 1997.
(5) Chung, T.-S., Ed. *Thermotropic Liquid Crystal Polymers*; Technomic: Lancaster, 2001.
(6) Ishida, H.; Kaji, H.; Horii, F. *Macromolecules* **1997**, *30*, 5799. Related references of liquid crystalline polymers are therein.
(7) Ishida, H.; Horii, F. *Macromolecules* **2001**, *34*, 7751.
(8) Liquid crystallization corresponds to the phase transition from the isotropic melt to the LC phase. In this paper such terminology is employed for simplicity instead of isotropization or clearing observed on heating.
(9) Ishida, H.; Horii, F. *Macromolecules* **2002**, *35*, 5550.
(10) Iimura, K.; Koide, N.; Tanabe, H.; Takeda, M. *Macromol. Chem.* **1981**, *182*, 2569.
(11) Torchia, D. A. *J. Magn. Reson.* **1981**, *44*, 117.
(12) (a) Gan, Z. *J. Am. Chem. Soc.* **1992**, *114*, 8307. (b) Hu, J. Z.; Orendt, A. M.; Alderman, D. W.; R. J., P.; Ye, C. H.; Grant, D. M. *Solid State Nucl. Magn. Reson.* **1994**, *3*, 181.
(13) Kaji, H.; Fuke, K.; Horii, F. *Macromolecules*, in press.
(14) Blumstein, R. B.; Stickles, E. M.; Gauthier, M. M.; Blumstein, A.; Volino, F. *Macromolecules* **1984**, *17*, 177.
(15) Percec, V.; Nava, H. *J. Polym. Sci., Part A: Polym. Chem.* **1987**, *25*, 405.
(16) Tonelli, A. E. *NMR Spectroscopy and Polymer Microstructure: The Conformational Connection*; VCH Publishers: New York, 1989.
(17) Ishida, H.; Maekawa, Y.; Horii, F.; Yamamoto, T. *Polym. Prepr., Jpn* **2001**, *50*, 2342.
(18) Maple, J. R.; Hwang, M.-J.; Stockfisch, T. P.; Dinur, U.; Waldman, M.; Ewig, C. S.; Hagler, A. T. *J. Comput. Chem.* **1994**, *15*, 162.
(19) Horii, F.; Beppu, T.; Takaesu, N.; Ishida, M. *Magn. Reson. Chem.* **1994**, *32*, 30.
(20) Horii, F. NMR Relaxations and Dynamics. In *Solid State NMR of Polymers*; Ando, I., Asakura, T., Eds.; *Stud. Phys. Theor. Chem.* Vol. 84; Elsevier Sci.: Amsterdam, 1998.
(21) Ernst, R. R.; Bodenhausen, G.; Wokaun, A. *Principles of Nuclear Magnetic Resonance in One and Two Dimensions*; Clarendon Press: Oxford, 1987.
(22) Horii, F. *Bull. Inst. Chem. Res., Kyoto Univ.* **1992**, *70*, 198.
(23) Duncan, T. M. *A Compilation of Chemical Shift Anisotropies*; Farragut Press: Chicago, 1990.
(24) Murphy, P. B.; Taki, T.; Gerstein, B. C.; Henrichs, P. M.; Massa, D. J. *J. Magn. Reson.* **1982**, *49*, 99.
(25) Fleming, W. W.; Fyfe, C. A.; Kendrick, R. D.; Lyerla, J. R.; Vanni, H.; Yannoni, C. S. *Polymer Characterization by ESR and NMR*; Woodward, A. E., Bovey, F. A., Eds.; *ACS Symp. Ser.* **1980**, *No. 142*, 193.
(26) Pines, A.; Gibby, M. G.; Waugh, J. S. *Chem. Phys. Lett.* **1972**, *15*, 373.
(27) Van Dogen Torman, J.; Veeman, W. S. *J. Chem. Phys.* **1978**, *68*, 3233.
(28) VanderHart, D. L. *J. Chem. Phys.* **1976**, *64*, 830.
(29) Opella, S. J.; Waugh, J. S. *J. Chem. Phys.* **1977**, *66*, 4919.
(30) Earl, W. L.; VanderHart, D. L. *Macromolecules* **1979**, *12*, 762.
(31) Tokita, M.; Osada, K.; Watanabe, J. *Liq. Cryst.* **1997**, *23*, 453.
(32) Ishida, H.; Maekawa, Y.; Horii, F.; Yamamoto, T. *Polym. Prepr., Jpn* **2002**, *51*, 1933.

MA025963S